Spatio-temporal refinement for InSAR phase unwrapping using untrained neural networks

Idi Boubacar-Sani[1,2], Xiaoran Jiang[1], Seynabou Toure[2], Kidiyo Kpalma[1], Oumar Diop[2], and Amadou-Seidou Maiga[2]

[1]*Univ Rennes, INSA Rennes, CNRS, IETR-UMR 6164, F-35000 Rennes, France*
[2]*Gaston Berger University, Saint-Louis, Senegal*
[1]*name.surname@insa-rennes.fr*
[2]*name.surname@ugb.edu.sn*

***Abstract*—Synthetic aperture radar interferometry (InSAR) enables high-precision ground deformation detection by measuring phase differences between SAR images. However, the challenging phase unwrapping is required to resolve inherent ambiguities. Disturbances like spatio-temporal decorrelation, atmospheric artifacts and multipath interference introduce noise, leading to unwrapping errors that affect ground motion estimation accuracy. In order to correct InSAR phase unwrapping errors made by traditional phase unwrapping methods, we propose utilizing an untrained deep neural network combined with early stopping during the learning process to more effectively capture the spatio-temporal priors of InSAR time series. Our model is untrained, meaning that it is learned only on the noisy wrapped InSAR data to be processed, without requiring any additional training data. Experimental results show that our method achieves competitive results compared to the European Ground Motion Service (EGMS) product and the reference methods.**

***Index Terms*—Untrained neural networks, InSAR, Phase Unwrapping, Time Series.**

I. Introduction and related works

By computing and analyzing interferograms that represent phase differences between Synthetic Aperture Radar (SAR) images of the same area taken at different times, techniques of Synthetic Aperture Radar Interferometry (InSAR) enable to reveal the evolution of ground deformation with high precision. However, several disturbance factors as spatio-temporal decorrelation and atmospheric artifacts can introduce noise, complicating 2D Phase Unwrapping (2DPU) and posing a significant challenge for InSAR applications. Indeed, with this acquisition noise, most of the traditional 2DPU methods tend to fail, either spatially, where strong phase variations between nearby pixels violate Itoh's condition (requiring phase differences to not exceed π [1]), or temporally, causing abrupt phase jumps in InSAR time series.

2DPU methods can be classified into three main categories [2]: path-following-based methods [3], [4], optimization-based methods [5] and those incorporating denoising process [6]. With the rapid advancement of deep learning, data-driven phase unwrapping methods have also been proposed. Among them, [7] estimates the phase discontinuities and applies them as cost functions for the minimum cost flow (MCF) solver of the method SNAPHU [18] to unwrap SAR interferograms. The works in [8], [9] treat InSAR phase unwrapping as semantic segmentation problems. However, most of these learning-based methods necessitate substantial amounts of training data.

Inspired by the concept of deep image prior [10], untrained neural networks [14], [16], [17] have been designed to solve image and video inverse problems, frame prediction and compression. Particularly, this approach has been used for phase unwrapping on biological data [11] that are not easy to acquire in large quantities and on InSAR data [19]. Despite good unwrapping accuracy, these works [11], [19] only leverage on spatial priors of an individual interferogram, without exploiting temporal priors in interferogram time series. Nevertheless, temporal coherence is crucial for applications such as ground motion detection and tracking.

In this paper, we propose a novel approach to improve spatio-temporal InSAR phase unwrapping by using an untrained and under-parameterized neural network, in which a latent-level temporal code generator is cascaded with an image-level spatial generator. The first acts as a good InSAR temporal prior, whereas the second as an InSAR spatial prior. This complementarity enables our model to consistently remove phase unwrapping errors in the time series of unwrapped interferograms. Our model is untrained in the sense that we do not need any training dataset. Network parameters are learnt only using as guidance the unwrapped and error-prone interferograms generated by a conventional phase unwrapping method. As a consequence, the network should necessarily be under-parameterized to allow regularization and avoid overfitting to the guidance interferogram sequence.

II. Background: Raw SAR data processing

Synthesized from the radar signal transmitted and received by a satellite antenna, the SAR images are complex data containing amplitude and phase. The amplitude generally varies because, on the ground, the emitted wave is reflected, transmitted or scattered, depending on the properties of the terrain. The phase consists of two main components: pixel phase and path phase. The latter is proportional to the sensor's wavelength and contains ground deformation information, which is the focus of this study.

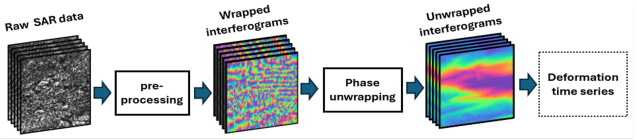

(a) The main SAR data processing workflow

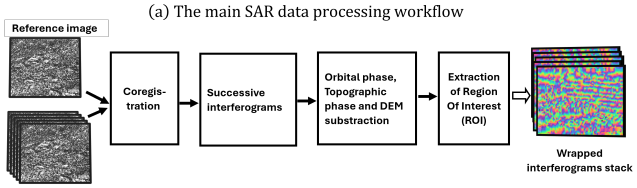

(b) Raw SAR data pre − pocessing workflow

Fig. 1. Illustration of raw SAR data processing workflow.

A. SAR data pre-processing

Extracting this ground deformation information involves applying multiple processing steps to raw SAR images. Figure 1(a) indicates the main data processing chain to finally extract univariate time series of ground deformation given raw InSAR path phase data, whereas Figure 1(b) details the steps of pre-processing, which consists in obtaining wrapped interferograms from raw data. In this work, we use SNAP (Sentinel Applications Platform) software [25] to perform this pre-processing. Raw SAR images of the same area acquired at different times are back-geocoded, which spatially aligns all these images to a single reference image, ensuring precise pixel-by-pixel correspondence. Interferograms are then generated, which are differences between the phases of the acquired consecutive back-geocoded images, respectively, at instants i and $i+1$. If φ_i and φ_{i+1} denote the phase at pixel p at instant i and $i+1$ respectevely, then this pixel will exhibit a phase shift $\Delta\varphi(p,i) = \varphi_{i+1} - \varphi_i$ in the interferogram, which reflects the ground deformation occurred between the two acquisition times. $\Delta\varphi$ is zero if the difference in the wave's round-trip distance between the target and the satellite is either zero or an integer multiple of the radar's half wavelength. Otherwise, $\Delta\varphi \in]0, 2\pi[$.

Substracting the digital elevation model (DEM), the topography contribution and the orbital phases from these interferograms, gives the phase representing terrain deformation. However, the noise due to disturbance like spatio-temporal decorrelations and atmospheric artifacts affects conventional phase unwrapping methods, leading to unwrapping errors that compromise the accurate evaluation of terrain deformation.

B. Phase unwrapping

Let us consider now ψ and ϕ the wrapped and unwrapped phases respectively, of a given interferogram. For each pixel p, the unwrapped phase ϕ can be derived from the wrapped one ψ, following the equation

$$\phi(p) = \psi(p) + 2k(p).\pi. \tag{1}$$

The aim of phase unwrapping operation is to find the appropriate integer value of $k(p) \in \mathbb{Z}$ for each pixel p.

However, this task is often prone to errors caused by SAR acquisition noise and inaccuracies in the unwrapping algorithms themselves. These errors, known as residues, arise when the sum of the phase gradients between four adjacent pixels in an interferogram is non-zero. Even a small percentage of residues in ψ can lead to significant variations in ϕ, resulting in violations of Itoh's condition.

III. Proposed Method

A. Overview

In this paper, we propose a novel neural model learnt in an untrained fashion, which effectively corrects unwrapping errors and preserves the space-time structure of InSAR phases. Our model is untrained in the sense that it is learned only on the noisy wrapped InSAR data to be processed, without any additional training data, labeled or unlabeled. Via network inference, it transforms a randomly generated three-dimensional tensor $\mathbf{Z} \in \mathbb{R}^{h_0 \times w_0 \times k_0}$ into a temporal sequence of unwrapped interferograms, which can be represented as a three-dimensional tensor $\mathbf{T} \in \mathbb{R}^{l \times h \times w}$ with l being the length of the sequence and $h \times w$ being the spatial resolution of each unwrapped interferogram.

Figure 2 illustrates the general architecture of our model that consists of three main components: a traditional phase unwrapping method as guidance, an image-level spatial generator $\mathcal{G}_I$ and a recurrent gated neural network-based temporal generator working on the latent code space denoted by $\mathcal{G}_C$.

The random input tensor $\mathbf{Z}$ is split into 2 parts: $\mathbf{Z}_s \in \mathbb{R}^{h_0 \times w_0 \times k_s}$ and $\mathbf{Z}_v \in \mathbb{R}^{h_0 \times w_0 \times k_v}$, with $k_s + k_v = k_0$. The former is dedicated to generating static phase information, while the latter is used for temporal phase variations. The tensor $\mathbf{Z}_v$ is first fed into the code-level temporal generator $\mathcal{G}_C$, which outputs a latent code sequence $\mathbf{C} \in \mathbb{R}^{l \times h_0 \times w_0 \times k_v}$, i.e. $\mathbf{C} = \mathcal{G}_C(\mathbf{Z}_v)$, each slice $\mathbf{C}_i$ with dimension (h_0, w_0, k_v) being a latent code at a given instant i. Note that the inference via $\mathcal{G}_C$ does not change the spatial dimension (h_0, w_0) and the channel dimension k_v of the tensor. It works as a temporal latent code generator by transforming a single random spatial code into a code sequence that encapsulates the temporal variations of an InSAR time series.

Then, each generated code slice $\mathbf{C}_i \in \mathbb{R}^{h_0 \times w_0 \times k_v}$ in $\mathbf{C}$, which captures temporal variations, is concatenated along the channel dimension with $\mathbf{Z}_s \in \mathbb{R}^{h_0 \times w_0 \times k_s}$ encapsulating spatial information to form a new code slice $\mathbf{C}'_i \in \mathbb{R}^{h_0 \times w_0 \times k_0}$. Note that $\mathbf{Z}_s$ is shared across all time instants, as we assume that unwrapped phase images in an InSAR time series are highly correlated and share consistent spatial information for stable regions unaffected by ground deformation. The resulting four-dimensional code volume $\mathbf{C}' \in \mathbb{R}^{l \times h_0 \times w_0 \times k_0}$ is then fed into the image-level generator $\mathcal{G}_I$ to output the unwrapped InSAR sequence, represented by the tensor $\mathbf{T} \in \mathbb{R}^{l \times h \times w}$. Note that the channel dimension k of the output tensor is reduced to 1, since interferograms are single-channel images.

During the learning process, the network's output is guided by a tensor $\mathbf{T_g} = [f_u(\mathbf{I}^1), f_u(\mathbf{I}^2), ..., f_u(\mathbf{I}^l)]$, where the unwrapped interferograms $f_u(\mathbf{I}^i)$ are stacked up. The notation $f_u(\mathbf{I}^i)$ denotes the phase unwrapping result using a conventional phase unwrapping algorithm f_u performed on

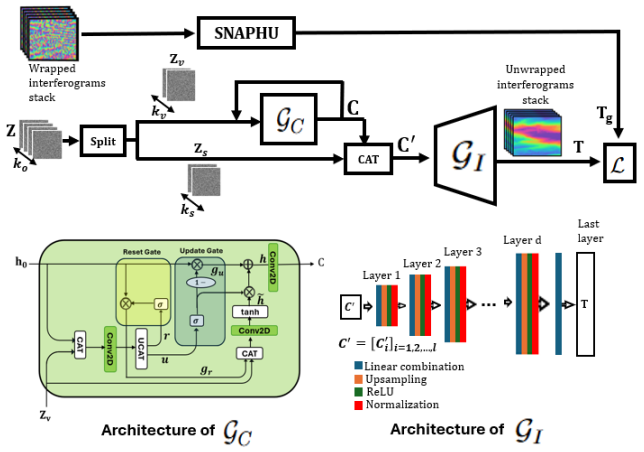

Fig. 2. Overview of the proposed untrained neural networks architecture for spatio-temporal refinement of unwrapped InSAR phase time series.

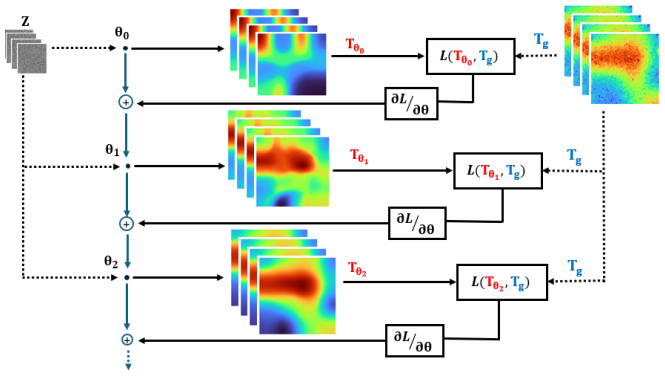

Fig. 3. Illustration of the network learning. $\mathbf{Z}$ denotes the input noise tensor, which is processed through the network with weights θ updated at each iteration, to generate the output $\mathbf{T}_\theta$. Gradient descent is performed to optimize θ by minimizing the loss function $\mathcal{L} = \|\mathbf{T}_\theta - \mathbf{T_g}\|$. An early stopping is performed to avoid overfitting to the guidance sequence $\mathbf{T_g}$.

the wrapped interferogram $\mathbf{I}^i$. This phase unwrapping is performed per image, without temporal constraint. Note that the obtained guidance unwrapped images are generally of low quality, spatially noisy and temporally inconsistent.

Overall, the whole network $\mathcal{G} = \{\mathcal{G}_C, \mathcal{G}_I\}$ is optimized by minimizing the following loss function:

$$\begin{aligned}\mathcal{L}_{\mathcal{G}_C,\mathcal{G}_I} &= \|\mathbf{T} - \mathbf{T_g}\| \\ &= \|\mathcal{G}_I(\mathcal{G}_C(\mathbf{Z}_v), \mathbf{Z}_s) - \mathbf{T_g}\|\end{aligned} \tag{2}$$

with $\|.\|$ denoting L2-norm.

It is important to note that in the same vein as conventional phase unwrapping algorithms, our model is said "untrained" since the learning is performed only given the initial wrapped interferograms $[\mathbf{I}^1, \mathbf{I}^2, ..., \mathbf{I}^l]$. No additional labeled or unlabeled training data is required. As a consequence, our method can be directly plugged onto any conventional phase unwrapping algorithm, while most of the deep learning based phase unwrapping models fail when training data is lacking.

The learning process of our network is illustrated in Figure 3. An early stopping is performed to avoid overfitting to the guidance sequence $\mathbf{T_g}$.

B. Conventional phase unwrapping as guidance

We use a conventional phase unwrapping method as guidance in our method. This method is applied independently to each image in the wrapped interferogram stack before passing them to our neural model. Several phase unwrapping methods [1], [3], [5], [13], [18] are assessed as candidates for guidance. The comparison of these methods are made on real-world and synthetic phase-wrapped data for which the unwrapped ground truth is available at [22]. The method SNAPHU [18] is finally chosen as our guidance since it provides more temporal consistency in the unwrapped interferograms than other candidate methods, despite some evident errors.

C. Image generator as InSAR spatial prior

Similar to [14], we adopt a decoder-like architecture which transforms a stack of low-dimensional latent codes $\mathbf{C}' \in \mathbb{R}^{l\times h_0\times w_0\times k_0}$ into high-dimensional unwrapped interferograms $\mathbf{T} \in \mathbb{R}^{l\times h\times w}$. Each network layer, except the last layer, includes several operation units: pixel-wise linear combinations (1×1 convolutions), upsampling operations, ReLU operations, and channel-wise normalizations. Upsampling $\times 2$ is performed at each layer to progressively increase the spatial resolution of the intermediate output tensor from $h_0 \times w_0$ to $h \times w$. Channel normalization enables fast and robust model learning. Finally, 1×1 convolutions are adopted to keep the number of network parameters sufficiently small. The under-parameterized nature of our generator enables efficient regularization of the refinement process and avoids overfitting while the network parameters are learned only using error-prone guidance interferograms. In the last layer, only the linear combination unit is applied to obtain the output tensor.

It is observed in our experiments that this structure efficiently removes phase unwrapping errors made by the conventional phase unwrapping algorithm SNAPHU. However, performing refinement independently on each of the InSAR images in the time series can result in temporal inconsistency (c.f. Figure 5). This is why we choose to combine the image-level generator with a code-level recurrent neural network, enabling our model to efficiently capture both the spatial and temporal prior of InSAR time series at the same time.

D. Code sequence generator as InSAR temporal prior

We employ Gated Recurrent Unit (GRU) to model the temporal prior in InSAR time series. The choice to use GRU in our work is primarily driven by its simple structure, which includes only two gates (update and reset), compared to Long Short-Term Memory (LSTM), which has three gates (input, forget, and output). This streamlined architecture of GRU allows for faster optimization during model learning, thanks to fewer network parameters. Similar to the image generator architecture, 1×1 convolutions are employed to maintain a low parameter count, thereby reducing the risk of overfitting.

IV. Experiments

A. Experimental data

1) Synthetic data: In our experiments, the synthetic test data is downloaded from [22]. These wrapped phase images are of spatial resolution 128×128 and are originally noise-free. Gaussian noises of standard deviation $\sigma = 1.6$ are then applied. Since these synthetic wrapped phase images are not part of a time series, we use them to evaluate the spatial refinement capability of our model, leveraging the availability of ground truth data.

2) Real-world data: The open-access policy of Sentinel-1 data is the primary reason for its selection in our study. Furthermore, Sentinel-1 provides several advantages, such as its frequent revisit time (6 to 12 days), its ability to acquire data under all weather conditions and its short C-band wavelength ($\lambda = 5.6$cm), which enables the detection and measurement of even minor ground deformations.

Experiments are conducted on areas of around 52km^2 in France. For each of these areas, 28 raw SAR images of resolution 128×128 (multilooking) from the Sentinel-1 archive [23] are downloaded, covering the period from January 2022 to December 2022. For each studied area, 27 wrapped interferograms are then obtained from these 28 raw SAR images by following the SAR data pre-processing steps described in Figure 1(b). These interferograms are then individually unwrapped by the conventional method SNAPHU by using the software snaphu-v2.0.7 (the latest version [24] released on February 2024) and sorted in chronological order before being fed to our model as data guidance. We also use EGMS product to extract unwrapped phases, which are considered as baseline.

B. Experiments and results

To assess the effectiveness of our method, two different approaches to perform phase unwrapping and refinement are studied on parallel. The first approach consists in learning a spatial generator per interferogram, without the code-level sequence generator performing temporal regularization. The second approach follows the complete processing framework described in Section III-A. An early stopping is executed after 500 learning iterations. This number is determined empirically to ensure that the generated outputs closely approximate the unwrapped guidance while preventing the learned model from overfitting to this same guidance which is error-prone.

Figure 4 shows the resulting unwrapped interferograms when testing on synthetic data. The unwrapped phases obtained by our method appear to closely match the ground truth. While the strong noise in the test data significantly reduces the unwrapping performance of reference methods, our proposed approach remains capable of delivering accurate estimations.

Figure 5 shows the visual comparison of the unwrapped interferograms when applying to real-world data. Each column displays the obtained two successive unwrapped interferograms taken in a time series by using different methods. It can be observed that our complete model incorporating both the latent code-level temporal generator and the image-level spatial generator is capable to generate temporally consistent unwrapped phase images within a time series, while other methods lack this capability.

This capability of generating consistent unwrapped InSAR phases is also assessed in Figure 6, which displays the phase evolution across the time obtained by different methods. In order to generate these time series, we geocode all the interferogram sequences in the reference coordinate system CRS WS84, then re-project them into the CRS LAEA Europe ETRS89, the coordinate system where the measurement points in the EGMS product are projected. We compare our results against the calibrated EGMS product on the available measurement points. The results in Figure 6 show that our complete model (temporal code generator + spatial generator) can produce temporally consistent phase time series and match closely to the EGMS baseline. On the contrary, other methods generate inconsistency and large fluctuations across the time. Table I shows the errors in terms of RMSE when comparing different phase unwrapping methods against the EGMS baseline. Our partial model, despite only learning an image generator independently frame by frame, achieves lower errors than other reference methods. This performance is still significantly improved by using our complete model incorporating both the temporal and spatial generators, which obtains the lowest RMSE.

TABLE I
PERFORMANCE OF DIFFERENT METHODS COMPARED TO EGMS AS BASELINE IN TERMS OF RMSE (MIN, MEAN, MAX).

Methods	RMSE		
	Min ↓	***Mean*** ↓	***Max*** ↓
SNAPHU	61.68	68.18	74.36
GF+SNAPHU	49.52	53.63	57.89
BM3D+SNAPHU	17.05	26.43	39.27
TV-L1+SNAPHU	14.99	20.74	31.55
Ours (Image generator only)	10.68	18.20	26.76
Ours (complete model)	**1.84**	**8.37**	**20.23**

V. Conclusion

In this paper, we proposed an under-parametrized deep generative model combining an image generator and a recurrent network-based sequential code generator to correct spatio-temporal unwrapping errors in InSAR phase time series. Our model is untrained, meaning it requires no additional training data beyond the unwrapped phase data it aims to refine. Experimental results on both synthetic data and real-world data demonstrate that the proposed model effectively removes phase unwrapping errors and enhances temporal consistency. In future work, we will further investigate the use of this model in the applications of ground deformation detection.

References

[1] D. C. Ghiglia, "Two-Dimentional Phase Unwrapping: Theory," Algorithms, Softw., 1998.

[2] H. Yu, Y. Lan, Z. Yuan, J. Xu, and H. Lee, "Phase unwrapping in InSAR: A review," IEEE Geosci. Remote Sens. Mag., vol. 7, no. 1, pp. 40–58, 2019.

[3] R. M. Goldstein, H. A. Zebker, and C. L. Werner, "Satellite radar interferometry: Two-dimensional phase unwrapping," Radio Sci., vol. 23, no. 4, pp. 713–720, 1988.

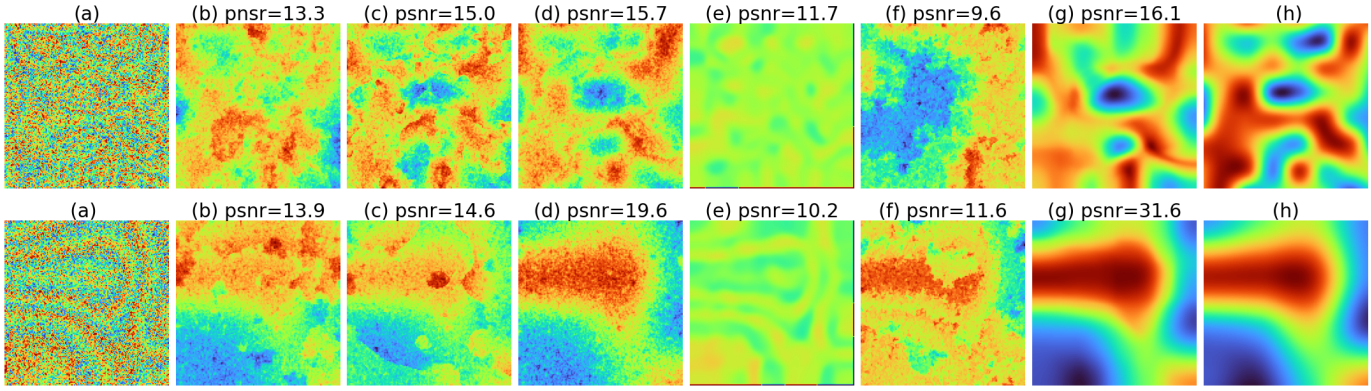

Fig. 4. Visual comparison of different InSAR phase unwrapping algorithms performed on test synthetic data. (a) Noisy wrapped phase, (b) Costantini [13], (c) Zhao et al [5], (d) SNAPHU [18], (e) BM3D [20]+SNAPHU, (f) TV-L1 [21]+SNAPHU, (g) Our model and (h) Ground truth.

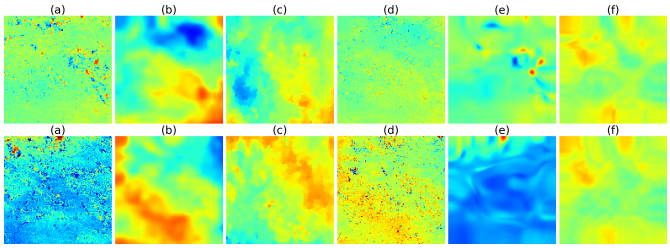

Fig. 5. Visual comparison of InSAR phase unwrapping of various techniques applied on real-world data. Each column shows two output successive images by using different methods. (a) SNAPHU [18], (b) BM3D [20] +SNAPHU, (c) TV-L1 [21] +SNAPHU,(d) GF(Goldstein Filter) [25]+SNAPHU, (e) our model with image generator only and (f) our complete model.

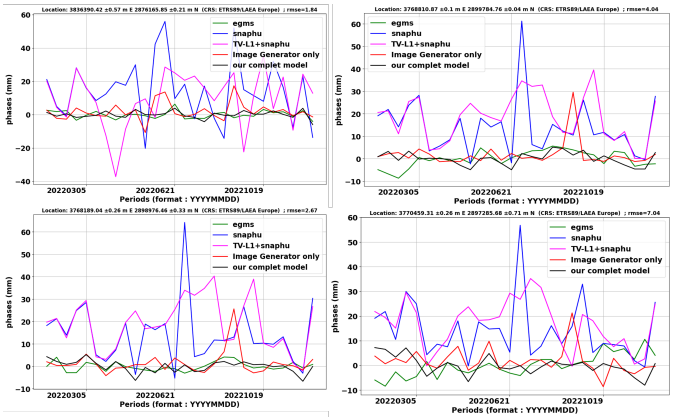

Fig. 6. Estimated time series of ground deformation at four different measurement points.

[4] T. J. Flynn, "Consistent 2-D phase unwrapping guided by a quality map," in Int. Geosci. and Remote Sens. Symposium, pp. 2057–2059, 1996.

[5] Z. Zhao, H. Zhang, Z. Xiao, H. Du, Y. Zhuang, C. Fan, and H. Zhao "Robust 2D phase unwrapping algorithm based on the transport of intensity equation," Meas. Sci. Technol., 30(1), 2018.

[6] R. Chen, W. Yu, R. Wang, G. Liu, and Y. Shao, "Integrated denoising and unwrapping of InSAR phase based on Markov random fields," IEEE Trans. Geosci. Remote Sens., vol. 51, no. 8, pp. 4473–4485, 2013.

[7] Z. Wu, T. Wang, Y. Wang, R. Wang, and D. Ge, "Deep-learning-based phase discontinuity prediction for 2D phase unwrapping of SAR interferograms," IEEE Trans. Geosci. Remote Sens., vol. 60, pp. 1–16, 2021.

[8] H. Wang, J. Hu, H. Fu, C. Wang, and Z. Wang, "A Novel Quality-Guided Two-Dimensional InSAR Phase Unwrapping Method via GAUNet," IEEE J. Sel. Top. Appl. Earth Obs. Remote Sens., vol. 14, pp. 7840–7856, 2021.

[9] L. Zhou, H. Yu, Y. Lan, and M. Xing, "Deep Learning-Based Branch-Cut Method for InSAR Two-Dimensional Phase Unwrapping," IEEE Trans. Geosci. Remote Sens., vol. 60, pp. 1–15, 2022.

[10] D. Ulyanov, A. Vedaldi, and V. Lempitsky, "Deep Image Prior," Int. J. Comput. Vis., vol. 128, no. 7, pp. 1867–1888, 2020.

[11] F. Yang, T. A. Pham, N. Brandenberg, M. P. Lutolf, J. Ma, and M. Unser, "Robust Phase Unwrapping via Deep Image Prior for Quantitative Phase Imaging," IEEE Trans. Image Process., vol. 30, pp. 7025–7037, 2021.

[12] S. Vijay Kumar, X. Sun, Z. Wang, R. Goldsbury, and I. Cheng, "A U-Net Approach for InSAR Phase Unwrapping and Denoising," Remote Sens., vol. 15, no. 21, pp. 1–17, 2023.

[13] M. Costantini, "A novel phase unwrapping method based on network programming," IEEE Trans. Geosci. Remote Sens., vol. 36, no. 3, pp. 813–821, 1998.

[14] R. Heckel and P. Hand, "Deep decoder: Concise image representations from untrained non-convolutional networks," arXiv Prepr. arXiv1810.03982, 2018.

[15] B. Y. Kiyakoglu and M. N. Aydin, "Unveiling the Significance of Individual Level Predictions: A Comparative Analysis of GRU and LSTM Models for Enhanced Digital Behavior Prediction," Appl. Sci., vol. 14, no. 19, p. 8858, 2024.

[16] A. Aich, A. Gupta, R. Panda, R. Hyder, M. S. Asif, and A. K. RoyChowdhury, "Non-adversarial video synthesis with learned priors," IEEE/CVF Conf. Comp. Vis. and Pat. Recog., pp. 6090–6099, 2020.

[17] X Jiang, J Shi, C Guillemot, "An untrained neural network prior for light field compression," IEEE Trans. Image Process., vol. 31, pp. 6922-6936, 2022.

[18] C. W. Chen and H. A. Zebker, "Phase unwrapping for large SAR interferograms: Statistical segmentation and generalized network models," IEEE Trans. Geosci. Remote Sens., vol. 40, pp. 1709-1719, 2002.

[19] A. Fejjari, G. Valentino, J. A. Briffa and R. A. Farrugia, "Convolutional deep learning network for InSAR phase denoising and unwrapping," Image and Signal Process. for Remote Sens. XXIX, 2023.

[20] K. Dabov, A. Foi, V. Katkovnik and K. Egiazarian, "Image Denoising by Sparse 3-D Transform-Domain Collaborative Filtering", IEEE Trans. Image Process., vol.16, pp. 2080-2095, 2007.

[21] A. Chambolle, V. Caselles, M. Novaga, D. Cremers and T. Pock, "An introduction to Total Variation for Image Analysis", hal-00437581, 2009.

[22] https://figshare.com/s/685e972475221aa3b4c4, [Last accessed: March 1, 2025].

[23] https://browser.dataspace.copernicus.eu/, [Last accessed: March 6, 2025].

[24] https://web.stanford.edu/group/radar/softwareandlinks/sw/snaphu/, [Last accessed: September 1, 2024].

[25] https://step.esa.int/main/download/snap-download/, [Last accessed: March 1, 2025].